Design of HOM Damped Multi-Cell SRF Cavities for CW Operation in High Current Storage Rings

Andranik Tsakanian, Adolfo Vélez, Emmy Sharples-Milne, and Jens Knobloch

***Abstract*—Currently, superconducting RF (SRF) systems for high-current storage rings are generally limited to low-frequency, moderate voltage, and single-cell cavities. For a new class of cavities to be used in longitudinal beam phase-space manipulation, high-voltage third harmonic multi-cell cavities are required, resulting in very challenging impedance considerations and higher-order mode (HOM) powers of the order of several kW per cavity. Thus, the cavity design requires far more attention on the HOM spectrum to be off-resonance with circulating beam harmonics. Special techniques have been developed to analyze the HOM spectrum and damping beyond the standard frequency range, which typically lies at a few GHz, as required by the VSR Demo project. Within the presented work, a four-cell 1.5 GHz cavity is designed including end-groups with multi-waveguide damping for a space-saving design capable of handling over 2.5 kW of HOM power per cavity. These cavities are designed for high-voltage operation with beam currents of at least 300 mA. Prototype systems are now in production. This article provides an overview of the advanced techniques for SRF cavity design and their application to tailoring the HOM spectrum and its application for the VSR Demo project.**

***Index Terms*—BESSY, eigenmode, electromagnetic fields, high energy accelerator, higher-order mode (HOM) damping, power, RF cavity, spectrum, storage ring, superconducting, wakefield.**

I. Introduction

SYNCHROTRON radiation sources have developed into highly sophisticated and reliable facilities that enable cutting-edge materials. From a user perspective, the photon beam parameters of interest are wavelength, flux, peak and average brilliance, coherence (longitudinal and transverse), and pulse length. Depending on the experiment being performed, the focus will lie on different parameters. A large and growing fraction of the BESSY II user community focuses on "functional materials" where dynamics in the picosecond and subpicosecond range are essential (e.g., magnetization dynamics for future information technologies), where the pulse length plays a major role.

At BESSY II, short pulses are provided during the dedicated low α operation periods or with the femto-slicing facility, albeit only at a small fraction of the photon flux provided during standard operation. Therefore, flux-hungry users are then literally left in the dark so that low α operation is limited to a few weeks per year. Nevertheless, an extensive user community focusing on dynamics research in the vacuum ultraviolet to soft X-ray range has developed, and the demand for increased short-pulse operation continues to grow rapidly. Thus, an important feature of future synchrotron sources will be the flexibility to tune the beam parameters to meet the various user needs, while ideally maintaining a high average flux.

The BESSY Variable Pulse Length Storage Ring (VSR) project [1], [2], [3] could serve as a future upgrade of the third-generation BESSY II light source. The technology developed also would pave the way for applications in newly developed fourth-generation light sources. VSR essentially is based on a strong periodic modulation of the accelerating voltage applied to different subsets of bunch buckets, generated by two groups of (typically two) superconducting cavities, resonating with 3rd and 3.5th harmonic of the base RF frequency. This approach places the highest demands on the design, fabrication, and operation of the multi-cell SRF cavities pushing the limits to new frontiers when compared to state-of-the-art developments in continuous wave (CW) high current systems. These challenges are recognized, and the development and demonstration of the required technology is the goal of the HZBs VSR Demo project [4]. In particular, two higher harmonics higher-order mode (HOM) damped cavity systems that will have to supply a CW voltage, by a factor of 20 higher than the base RF voltage, and therefore experience high peak fields of the order of 20 MV/m. They further need to interact with a high average current beam of 300 mA, which includes transients by one or more clearing gaps and some sets of single bunches to cover the needs of a modern synchrotron-based light source and user facility. For example, the BESSY VSR cavities would operate at an order of magnitude higher voltage than the fundamental SOLEIL cavities while accelerating a similar average beam current [5]. The same holds true for higher harmonic SRF systems, as presented in [6], or as they are used at SLS and ELETTRA [7]. More developments on passive harmonic SRF cavities are given, for example, in [8], [9], [10], and [11].

Received 23 January 2025; revised 20 March 2025; accepted 21 March 2025. Date of publication 26 March 2025; date of current version 25 April 2025. *(Corresponding author: Andranik Tsakanian.)*

Andranik Tsakanian and Emmy Sharples-Milne are with the Helmholtz-Zentrum Berlin für Materialien und Energie GmbH (HZB), Institute of Science and Technology of Accelerator Systems, 14109 Berlin, Germany (e-mail: andranik.tsakanian@helmholtz-berlin.de).

Adolfo Vélez is with the Helmholtz-Zentrum Berlin für Materialien und Energie GmbH (HZB), Institute of Science and Technology of Accelerator Systems, 14109 Berlin, Germany, and also with the Technische Universität Dortmund, 44227 Dortmund, Germany.

Jens Knobloch is with the Helmholtz-Zentrum Berlin für Materialien und Energie GmbH (HZB), Institute of Science and Technology of Accelerator Systems, 14109 Berlin, Germany, and also with the Universität Siegen, 57068 Siegen, Germany.

Color versions of one or more figures in this article are available at https://doi.org/10.1109/TASC.2025.3554959.

Digital Object Identifier 10.1109/TASC.2025.3554959

BESSY VSR requires the installation of multi-cell SRF higher harmonic cavities of the fundamental 500 MHz at two different frequencies. Therefore, four new SRF cavities (2 × 1.5 GHz and 2 × 1.75 GHz) are designed [12], [13], [14], [15], [16], [17]. The aforementioned requirements made the cavity design challenging, particularly since stable operation is paramount. Thus, special attention was paid to the damping of the HOMs, which are excited by the high current circulating beam and may lead to coupled bunch instabilities. Therefore, the cavity design requires extreme care in handling the HOM spectrum to ensure it is off-resonance with circulating beam harmonics. The design solution presented in this article describes the design steps required to fulfill the impedance specifications imposed by the VSR Demo project cavities.

The state-of-the-art techniques based on eigenmode calculations are by definition limited in frequency due to convergence issues. In the case of high current storage ring applications, this represents a major showstopper since the risk of beam loss due to impedance at higher frequencies is high. To overcome this problem this article successfully applies the Prony–Pisarenko pole fitting technique and wakefield simulations as an alternative to conventional methods to extend the HOM spectrum calculations beyond four times the standard approach for this particular cavity. Due to the highly populated HOM spectrum of multi-cell cavities at higher frequencies, the high risk of coincidence of an HOM with a beam revolution harmonic imposes the need to achieve some level of control over the HOM frequencies. In this work, the impact of the cell-shape parameters has been revisited and the main parameters with an effect on the HOM spectrum response have been identified. As a result, dangerous HOM modes can, with some limitations, be tuned away from undesired frequencies while simultaneously conserving the fundamental pass-band specifications (frequency, field flatness).

In this article, the electromagnetic design of those strong HOM-damped SRF cavities is presented. In addition, the application and limitations of different numerical techniques for the evaluation and control of the HOM spectrum of the cavities are discussed. Detailed attention was paid to the filling pattern of the circulating bunches in the BESSY II storage ring [1], [2], [3]. Consequently, the development of a new design mechanism to tailor the cavity broadband HOM spectrum in the design stage was implemented. This is of particular importance when fulfilling its off-resonance condition with the prominent spectral components of the circulating high current beam.

This article is organized as follows.

1) In Section II, the concept of the BESSY VSR is presented. The physics case of the third harmonic RF upgrade of the operating BESSY II storage ring is discussed.
2) In Section III, the concept of strong HOM-damped SRF cavities is presented.
3) Section IV covers the design aspects of the SRF cavity including a detailed definition of the design criteria for the accelerating mode (AM) and HOMs, a description of an advanced multi-stage geometry optimization scheme, fundamental mode tuning, and eigenmode simulations.
4) In Section V, the broadband HOM spectrum control technique is presented. It covers the topics of long-range wakefield simulations and resonant mode extraction by advanced pole-fitting methods, HOM spectrum shift analyses, and a derivation of the geometry parameters sensitive for the HOM spectrum tuning.
5) In Section VI, the HOM power levels and spectrum for the BESSY VSR 300 mA current filling pattern are presented. The HOM power distribution and extraction from the cavity are discussed.
6) In Section VII, the work is summarized, key points are highlighted, and future applications are discussed.

TABLE I
BESSY II STORAGE RING PARAMETERS

Lattice	DBA
Circumference	240 m
Energy	1.7 GeV
Current	300 mA
RF frequency	500 MHz
Bunch length	15 ps
Revolution time	800 ns
Number of RF buckets	400
Emittance	6 nm rad

II. CONCEPT OF BESSY VSR

The realization of the BESSY VSR project implies the installation of a single superconducting module with four cavities in one of the low beta straight sections of the existing BESSY II storage ring (Table I).

The concept relies on 1.5 GHz CW superconducting RF (SRF) cavities to provide 80 times more longitudinal focusing than the normal conducting RF system in BESSY II. The additional installation of a second 3.5 harmonic SRF system (1.75 GHz) leads to a beating of the induced cavity voltages while bunches can be compressed by roughly a factor of $\sqrt{80}$ into the few picosecond range. Therefore, a combination of long and short buckets can be simultaneously generated. Then, long bunches can be stored to provide the high photon flux while only a few short-bunch buckets are populated with high charge for short-pulse experiments. This procedure avoids eventual impedance and Touschek lifetime problems. Fig. 1 shows the bunch length diagram versus single bunch current for the cases of BESSY II and VSR upgrade. As can be seen, the proposed VSR concept allows to store shorter bunches with high current and with low α operation to reach even shorter pulses down to a few hundred fs level.

The corresponding voltage beating in the time domain created by the three cavity systems (0.5 GHz, 1.5 GHz, and 1.75 GHz) is presented in Fig. 2. The voltage amplitudes of each third harmonic RF frequency are tuned to achieve cancelation of 1.5 GHz and 1.75 GHz voltages at even buckets and adding up at odd buckets corresponding to 16 MV and 14.14 MV, respectively. Thus, long bunches are placed within the low gradient buckets, while the short bunches appear 2 ns shifted.

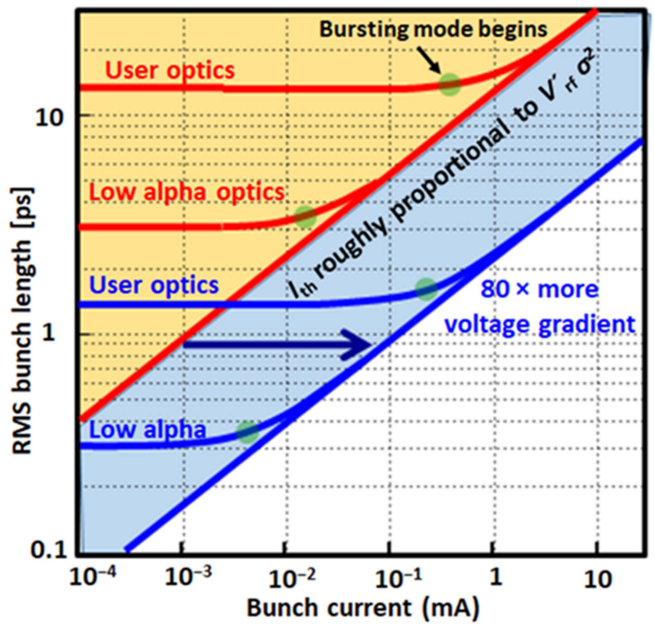

Fig. 1. Schematic bunch length current relation of BESSY II (red line) and the short bunches of BESSY VSR with upgraded RF focusing (blue line).

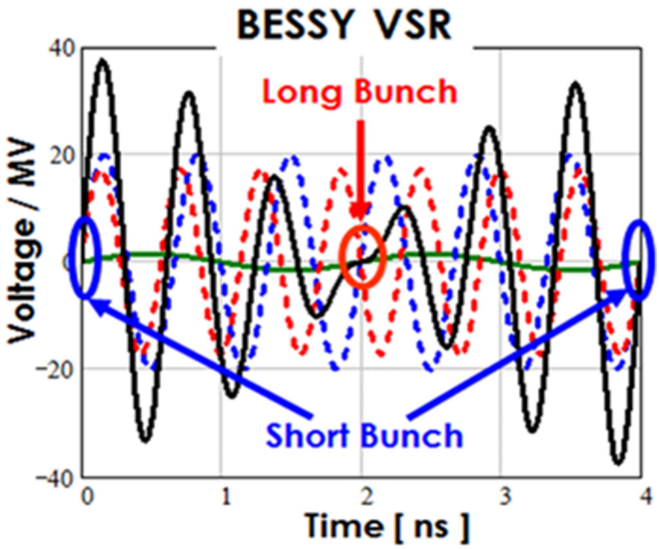

Fig. 2. Bunch fill pattern with long (red ellipse) and short (blue ellipse) bunches. The colored voltages correspond to the 500 MHz (green), 1.5 GHz (blue dashed), 1.75 GHz (red dashed), and the resulting sum voltage (black) defining the bucket sizes and locations.

The nominal BESSY VSR filling pattern of the 240 m circumference ring is shown in Fig. 3 where the short and long bunches will be stored simultaneously. In total, 400 RF buckets with 2 ns bunch spacing are available.

In this work, two types of bunch-filling patterns are considered: the so-called "Extended" shown in Fig. 3 and the "Baseline" with the omission of 150 short-pulse, low-charge bunches. The repetition rates of 500 MHz and 250 MHz are defined by bunch spacing in each pattern, respectively. Thus, the beam harmonics multiples of 250 MHz must be considered as prohibited resonant frequency lines imposing the cavity HOM spectrum to be off-resonance from those lines at any given time.

Ideally, the cavity HOM spectrum should also fulfill the off-resonance condition with respect to the circulating beam harmonics located at multiples of 1.25 MHz revolution frequency [3], [4], [5], [6], [7]. Unfortunately, the excitation spectrum of the bunches in the storage rings typically is very broad and covers more than 10 GHz, making it practically impossible to design even a single cell cavity not having HOM frequencies hitting the aforementioned harmonics. This argument applies also to all vacuum chambers of the storage ring components including the inner volumes of sealing flanges, which represent one of the main impedance sources causing overheating of accelerator components in a single bunch operation regime. Thus, in this mode, the ring stable operation imposes a significant current reduction down to 20 mA.

III. Concept of HOM Damped SRF Cavity

Due to the expected kW HOM power levels and in view of the very limited real-estate length available, the decision was made to use waveguide-damped cavities instead of beam pipe HOM absorbers. The chosen design was inspired by the prototype developed by Jefferson Lab [17], [18], [19] due to its compact design and the capability of the waveguides to transport a high amount of power far away from the cryogenic cavities toward water-cooled HOM loads at the waveguide ends [20]. This first worldwide prototype cavity was vertically tested (Q versus E) successfully without a Helium vessel. Nevertheless, the integration in a Helium vessel unfortunately did not follow and it became clear that the procedure would represent an engineering challenge. This topic is mainly of concern to the mechanical design of the cavity and will be addressed in a separate publication, but of course, poses an extra toll on the amount of EM design changes required to fulfill mechanical specifications. More importantly, as described in [17], [18], and [19], the impedance threshold achieved by this original prototype still does not meet the requirements for a synchrotron machine such as BESSY II. The complete design process had to be revisited which resulted in a complete design process flow.

As a result, the design of the VSR SRF cavities (Fig. 4) consists of four elliptical cells connected with two waveguide-end-groups where the five HOM waveguide (WG) dampers and a fundamental power coupler (FPC) port are located. The cavities are supplied with enlarged beam pipes (BmP), as compared to, i.e., multi-cell Tesla-type cavities, to reduce the cut-off frequency and favor an efficient HOM extraction. Of course, special attention was put to energy conservation of the TM_{010} fundamental π-mode. Although the beam tube apertures and WG-dampers cut-off frequencies are above the fundamental mode frequency, the field leaking of the fundamental mode into those parts was carefully considered. As discussed and depicted in Fig. 4, the HOM waveguides imply a transition from superconducting Niobium to stainless steel in an actively cooled flange at a distance of 320 mm from the cavity axis. Thus, evanescent field leaking into the joining flange could lead to Q-drops and possible quenches, so the field levels need to be

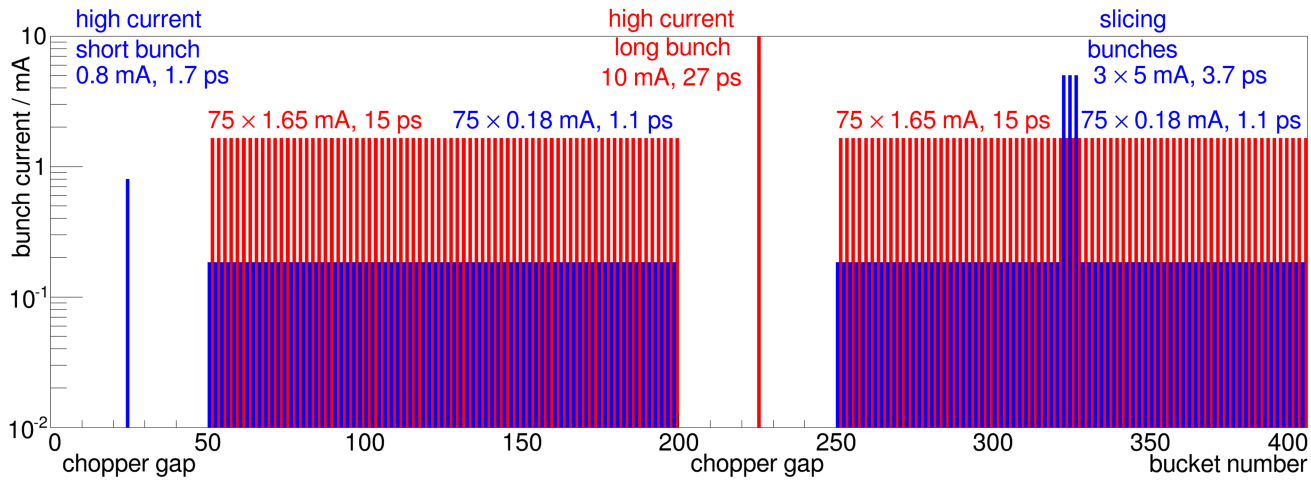

Fig. 3. BESSY VSR filling pattern including short (blue) and long (red) bunches.

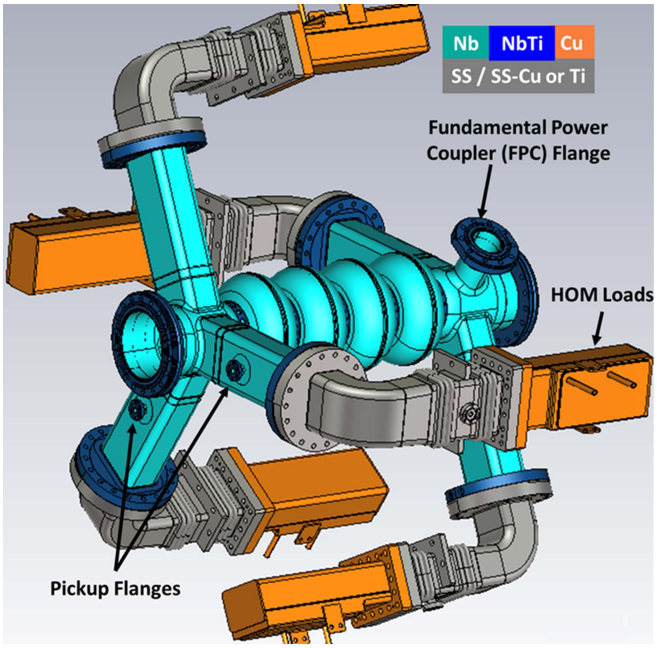

Fig. 4. General layout of the waveguide-damped four-cell VSR cavity.

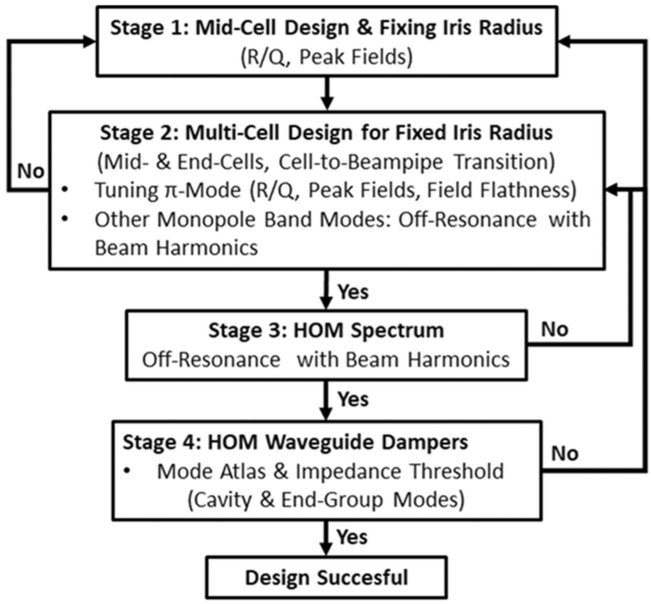

Fig. 5. Multi-stage optimization scheme of cavity design.

carefully computed. Hence, to preserve the high Q properties of the SRF cavity, the HOM waveguide extensions (up to the transitioning flange) should be long enough to remain superconducting under operating conditions. These HOM waveguides enable the placement of the pickup antennas for both the LLRF control and field evaluation purposes. Thus, they are designed to cover the signal levels (Qantenna $> 10^{11}$) required for the control.

IV. Design of the SRF Cavity

As expected, the design process to fulfill the cavity specifications results in a complicated multi-stage optimization process. To help understand the procedure a flow diagram is depicted in Fig. 5, where the accelerating π-mode frequency is considered as one of the key parameters.

As a starting point (stage 1), the basic mid-cell geometry must be identified, the iris radius is a key parameter that to be fixed for further optimization. In stage 2, the multi-cell cavity is constructed together with beampipes. The fine-tuning of the accelerating π-mode ensures that the requirements for the important RF parameters, such as R/Q, field flatness, and the peak electric and magnetic fields, are satisfied for high gradient operation at this stage. Other monopole band modes of the SRF cavity are damped only through the FPC port and can be excited strongly in the high-current storage ring. Thus, the off-resonance condition of those modes with beam harmonics (multiple to 1.25 MHz revolution frequency) is checked always and is considered an additional condition for π-mode tuning. Then, in stage 3, the

TABLE II
CRITERIA AND RF PARAMETER SENSITIVITY ON GEOMETRY PARAMETERS

Criteria	RF param.	Action	Geometry param.
High gradient (20 MV/m CW)	E_{pk}/E_{acc}	Dec.	$R_{ir.}$ – Dec., {a, b}
	B_{pk}/E_{acc}	Dec.	$R_{ir.}$-Dec., {A, B}
Low cryogenic losses	R/Q×G	Inc.	
Low HOM impedance	R/Q×Q_L	Dec.	$R_{ir.}$ – Inc.

cavity HOM spectrum (up to 20 GHz) off-resonance condition is checked with respect to the beam harmonics multiples to 250 MHz, ensuring the absence of any trapped mode in the cavity as well. Finally, in stage 4, the rectangular waveguides for HOM damping are constructed ensuring the preservation of accelerating π-mode RF parameters. Then, the HOM spectrum must be computed. Unfortunately, the eigenmode computations for structures with open ports get intrinsically difficult with an increasing number of propagating waveguide modes. Thus, solver convergence gets poor, and mode separation becomes ambiguous making it difficult to identify the type of the cavity mode being calculated. As a matter of practical experience, this regime is reached for the VSR cavity around 3 GHz. This article shows the possibility of extending this frequency mapping range above the 10 GHz frequency range by making use of the wake potential simulations instead of the conventional pure eigenmode approach. This is crucial to ensure that the off-resonance condition between the cavity HOMs and the circulating beam harmonics is fulfilled, otherwise, the cavity geometry parameters should be reconsidered. Once the optimum design is reached, in terms of the fulfillment of the HOM spectrum off-resonance condition with the circulating beam harmonics, the broadband HOM impedances should be controlled to not exceed the impedance threshold of the machine. Typically, the last stage can require additional optimization of the HOM damping waveguides for stronger damping, and eventually, the generation of localized end-group modes might require intermediate tapered sections to modify cut-off frequencies for different polarizations [12]. To design this kind of complex cavity, eigenmode, and wakefield simulations are executed and discussed in the next sections in more detail.

A. Mid-Cell Design (Stage 1)

The geometry parameters used in mid-cell design are presented in Fig. 6.

The first stage of an SRF high current cavity design consists of finding the mid-cell parameters that fulfill the RF specifications and offer the best possible performance in terms of gradient, losses, and impedance as depicted in Table II. In this table, the cell geometry parameters as defined in Fig. 6, the notations

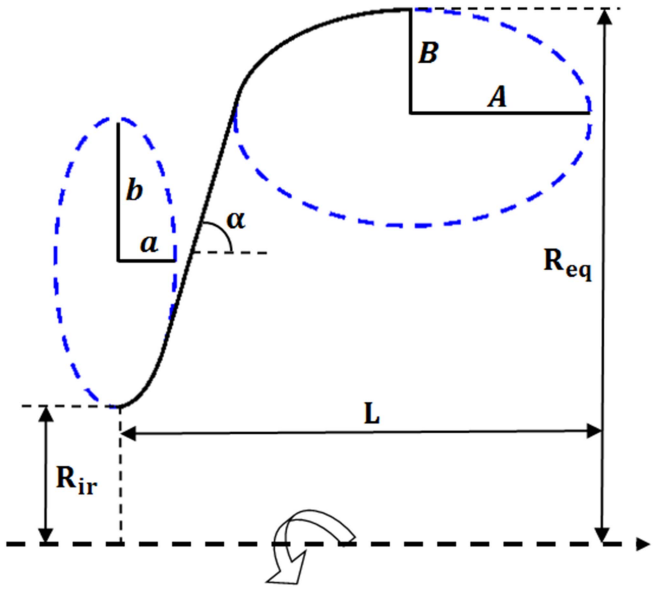

Fig. 6. Geometry parameters of a half-elliptical cell.

"Dec." for decrease and "Inc." for increase are used. The cell optimization of elliptical cell shapes requires the fine-tuning of six different geometry parameters (Fig. 6). This is done by CST eigenmode simulations. The optimization direction of each RF parameter is given in the column "Action" and the sensitive geometry parameters are listed in the last column. Decreasing the iris radius R_{ir} will decrease the peak fields and lower cryogenic losses while for HOM damping bigger R_{ir} is required. Thus, the cell design requires finding the best possible geometry parameters that fulfill the accelerating π-mode and the HOM low impedance requirements.

Naturally, the parameters defining the cell geometry are linked to one another, and therefore finding the best geometry becomes a long iterative process. Many intensive studies on cell optimization and sensitivity of the RF-cell geometry parameters have been performed for different SRF cavities and can be found, for example, in [21].

As the starting point for the mid-cell design of the 1.5 GHz cavity, the Cornell [22] and the JLab [19] designs were considered. As it was previously pointed out damping higher order modes is an important issue when designing an SRF cavity and in particular for the BESSY VSR project this aspect plays a crucial role. Thus, it is vital to ensure proper damping and avoid trapped modes inside the structure.

A general indicator of how easily the modes can be propagated along the structure is the coupling factor K, characterizing the electromagnetic coupling between adjacent cells. K is determined by the cell geometry, especially the diameter of the iris. The coupling factor is defined by

$$K = 2\frac{f_\pi - f_0}{f_\pi + f_0} \cdot 100\% \quad (1)$$

where f_π and f_0 represent the resonance frequency for the π and 0 modes, respectively. In our final design, the iris diameter has been increased to 70 mm. This value is slightly larger

TABLE III
COMPARISON BETWEEN RF DESIGN GOAL PARAMETERS FOR THE CORNELL (SCALED), JLAB, AND BESSY VSR MID-CELLS MODELS

Parameter	Cornell	JLab	HZB	Goal
E_{pk}/E_{acc}	2.06	2.43	2.26	< 2.5
B_{pk}/E_{acc} [mT/(MV/m)]	4.66	3.95	4.84	< 5.5
R/Q [Ω]	110.0	104.4	100.5	> 100
Geometry factor - G [Ω]	271.1	277.2	278.3	> 270
K for π-TM_{010} [%]	2.01	2.01	3.2	> 3
Iris diameter [mm]	62	68	70	

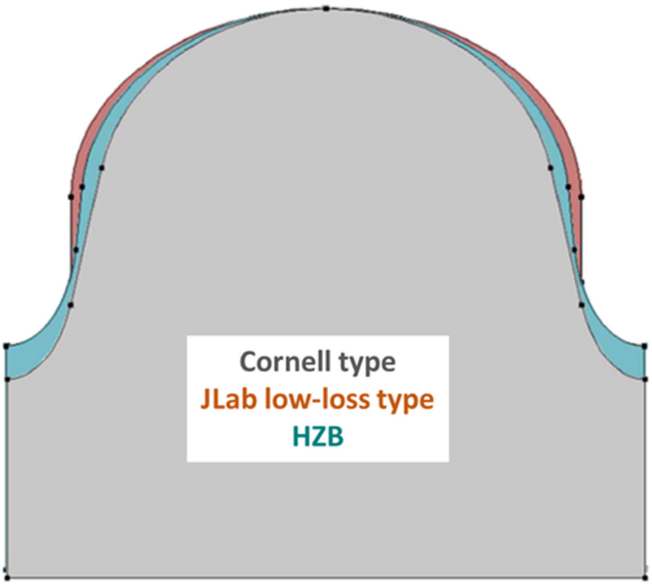

Fig. 7. Comparison between different base-model mid-cells and the HZB base layout.

than in JLab and Cornell models in order to obtain a higher cell-to-cell coupling factor for the fundamental mode as shown in Table III. This increase allows the most probable trapped modes to propagate more efficiently through coupling from the inner cells to the outer ones. A final set of mid-cell parameters fulfilling specifications has been obtained by performing parametric electromagnetic calculations with the main figures of merit (R/Q, G, E_{pk}/E_{acc}, and B_{pk}/E_{acc}) as a design goal for AM and the HOM spectrum off-resonant condition with beam harmonics of the BESSY II storage ring.

A comparison of the results obtained on the HZB mid-cell design with the characteristic parameters for the JLab and Cornell (scaled to 1.5 GHz) models are depicted in Table III and the cell contours are shown in Fig. 7. As can be seen, all the target RF specifications are fulfilled with a significant improvement of the coupling factor K in comparison to the base models.

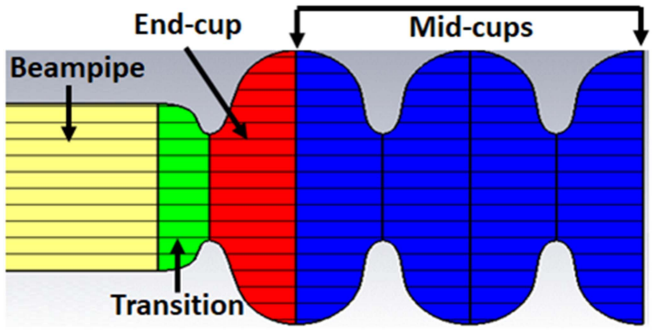

Fig. 8. Geometry layout of the multi-cell cavity.

More details on the mid-cell optimization are discussed in [12]. In conclusion, the mid-cell geometry obtained represents a good candidate as a base model for the whole four-cell cavity design. From now on the iris radius is assumed to be fixed at $R_{ir} = 35$ and 30.5 mm for 1.5 and 1.75 GHz BESSY VSR cavities, respectively. These values represent a compromise to maximize both the HOMs propagation and the accelerating gradients. The frequency of the AM is tuned by adjusting the equator radius, while the peak electric and magnetic fields are optimized by varying the geometry parameters of the iris and equator ellipses, respectively.

B. *Fundamental Mode Tuning for Multi-Cell Cavity (Stage 2)*

The design of the multi-cell cavity (Fig. 8) contains four elliptic cells for acceleration equipped with enlarged beampipes to allow for HOM propagation and prevent the cavity from trapping modes.

The criteria of peak electric field $E_{pk}/E_{acc} < 2.5$ and the peak magnetic field $B_{pk}/E_{acc} < 5.5$ mT/(MV/m) are always fulfilled [23], [24].

For the whole cavity analysis, an eigenmode-computing-based standard multi-cell optimization is performed to find the best RF parameters that fulfill the specifications for the multi-cell cavity while keeping the field flatness. The final optimized geometry parameters are presented in Table IV, where the half-cell is denoted as "cup." The geometry parameters follow the definition given in Fig. 6 for the mid-cells. The beam-pipe length is 0.25 m on both sides with a radius of 55 mm and 47 mm for the 1.5 GHz and 1.75 GHz cavities, respectively.

As previously mentioned, the beam-pipe apertures are designed to have cut-off frequencies above the cavity fundamental mode frequency but large enough so that HOM power is extracted out to the waveguide-loaded end groups. It is unavoidable that the fundamental TM_{010} leaks into the beampipe section decaying along its length. Thus, the beampipe lengths are defined so that this fundamental mode decays significantly before reaching the flange position to avoid causing a quench by insufficient cooling. The Q-drop due to the flange losses should be well below 1%. This available beampipe length allows for the implementation of the waveguide-loaded end-group principle, using waveguides for HOM damping and an FPC port. As presented in [12] and [18], the cut-off frequencies of those

TABLE IV
GEOMETRY PARAMETERS IN MM UNITS OF THE BESSY VSR 1.5 GHZ AND 1.75 GHZ (IN BRACKETS) CAVITIES

Parameter	Mid-cup	End-cup	Transition
R_{eq}	90.0 (77.2)		55.0 (47.0)
R_{ir}	35.0 (30.5)		
a	10.5 (9.0)		5.0 (4.5)
b	15.8 (14.1)		4.0 (3.5)
A	38.0 (33.0)	35.0 (30.3)	22.0 (15.0)
B	34.0 (29.1)		10.0 (8.5)
L	50.0 (43.0)		30.0 (27.0)

arms must be carefully analyzed to allow HOM propagation and fundamental mode preservation.

An important parameter in the design of multi-cell cavities is the field flatness, which is defined as follows:

$$\mu_{ff} = \left(1 - \frac{E_{\max} - E_{\min}}{\frac{1}{N}\sum_{i=1}^{N} E_{c,i}}\right) \cdot 100\% \qquad (2)$$

where $E_{c,i}$ is the peak axial accelerating field in ith cell of the multi-cell cavity of N cells and $E_{\max}$ ($E_{\min}$) the maximum (minimum) field among N cells. When $E_{c,i}$ is equal, the flatness is 100%.

The field flatness indicates the efficiency of the accelerating field distribution between the cavity cells and is tuned by the end-cups of both end-cells. During the cavity design and geometry optimization, intensive numerical studies were performed on the field flatness sensitivity of the different geometry parameters of the cavity. It is observed, that for a fixed iris radius the field flatness mainly depends on the equator ellipse parameter A of the mid- and end-cups. Thus, for a given R_{ir} the optimized ratio $A_{end\text{-}cup}/A_{mid\text{-}cup}$ will preserve the field flatness and does not depend on the variation of the other geometry parameters typically used for fine-tuning the AM frequency and related peak electric and magnetic fields on the cavity walls.

As a result, Fig. 9 depicts the field profile of the on-axis accelerating electric field of the 1.5 GHz cavity. The red dots in the field profile indicate the peak axial accelerating fields $E_{c,i}$, and 97% of field flatness was reached. It can be noted that the evanescent field outside the cavity cells (dashed lines in Fig. 9) is not negligible due to the enlarged beam-pipe radius. This will result in a slight reduction of the accelerating voltage occurring in the cavity cells with a total length of L_{active}. The decelerating amplitude of the evanescent fields does not depend on number of elliptical cells. For the four-cell cavity, the contribution to the total accelerating voltage degradation is about 4.5% while the R/Q is reduced by 8%. Still, the R/Q $>$ 100 Ω per cell design goal is fulfilled. Note, that increasing the number of cells will reduce the contribution of the evanescent field. In Table V, the final RF properties of the AM of the 1.5 GHz and 1.75 GHz cavities are summarized.

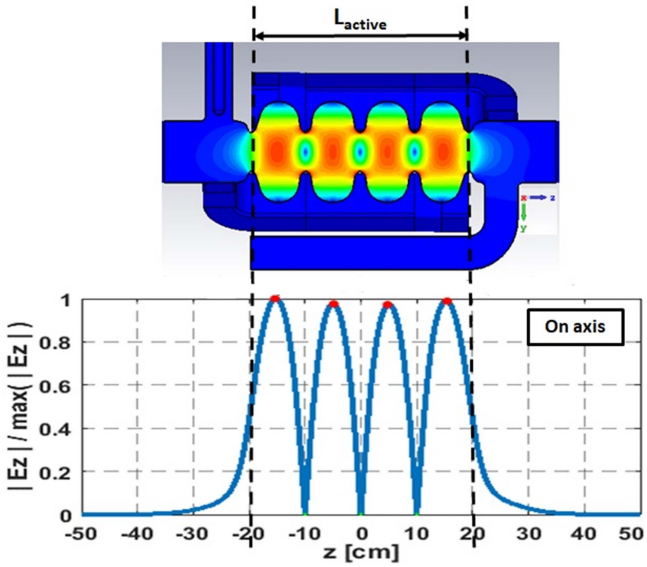

Fig. 9. On-axis electric field amplitude along the 1.5 GHz cavity and normalized $E_{c,i}$ field values (red dots). The reference length L_{active} is geometrically defined as the distance between the outermost cell irises.

TABLE V
RF PROPERTIES OF SRF CAVITIES

RF parameter (TM_{010} π-mode)	Cavity type		Design goal
	1.5 GHz	1.75 GHz	
Number of cells	4		4
Active length [m]	0.4	0.344	
Frequency [GHz]	1.4989	1.7489	3rd and 3.5th harmonic of 499.65 MHz
Q_{ext}	5×10^7	4.3×10^7	
Geometry factor - G [Ω]	277	275	> 270
E_{pk}/E_{acc}	2.32	2.30	< 2.5
B_{pk}/E_{acc} [mT/(MV/m)]	5.05	5.23	< 5.5
R/Q [Ω]	386	380	> 100 per cell
Field flatness - μ_{ff}	97 %	99%	> 95 %

Since the accelerating field is mainly concentrated in the cells, it is reasonable to define the accelerating gradient as follows:

$$E_{acc} = \frac{\left|\int E_z \cdot e^{j\frac{\omega}{c}z} dz\right|}{L_{active}} \qquad (3)$$

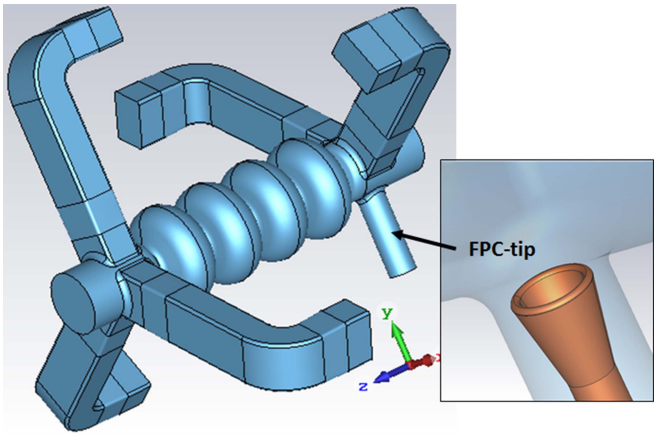

Fig. 10. General layout of the waveguide-damped four-cell VSR cavity (HOM loads not shown).

where E_z is the axial electric field of the AM with resonant frequency $f = \omega/2\pi$ and the field integration is along the entire cavity.

Due to the complexity of the HOM spectrum computation and possible control, a separate section is dedicated to this purpose. This is considered as part of the stages 3 and 4 (Fig. 5) and is described in the next section.

C. HOM Damping and Monopole Band Modes (Stage 2 and Stage 4)

To operate the SRF cavities in a high-current machine such as a storage ring it is critical to ensure that the impedances of all the cavity modes remain below the active feedback threshold of the machine. In this case, the feedback threshold for BESSY II was measured [25] to be 5×10^4 Ω and 10^7 Ω/m for the longitudinal and transverse impedances, respectively. These feedback thresholds should be considered as impedance budget limits for the entire machine, where the RF cavities have a significant contribution. Hence, accurate calculations of the complete set of cavity resonant modes within a specified frequency range, a so-called mode atlas, are essential.

As introduced the strong damping concept relies on the integration of five rectangular waveguides located on the beampipes on both sides of the cavity (Fig. 10). The rectangular waveguides in each end-group are rotated by 120° with respect to each other and the end-groups are rotated by another 60° in addition to capture the cavity HOMs with different polarizations. The cut-off frequencies of those waveguides are above the cavity AM frequency enabling them to be located closer to the cavity cells for stronger damping. The waveguide cross section is set to 60 $\times$ 95 mm^2 and 60 $\times$ 84 mm^2 for 1.5 GHz and 1.75 GHz cavities, respectively. The corresponding cut-off frequencies for the TE_{10} waveguide mode are 1.577 GHz and 1.784 GHz, respectively. A detailed study showed the possibility of creating end-group localized modes below the waveguide cut-off. Thus, to improve the HOM propagation in the waveguides and provide strong damping of those HOMs, two 50 mm long tapers are introduced in the rectangular WGs lines with the cross-section change: 60 $\times$ 88–91 mm^2, 60 $\times$ 91–95 mm^2 and 60 $\times$ 76–78 mm^2, 60 $\times$ 78–84 mm^2 for the 1.5 GHz and 1.75 GHz cavities, respectively. Since the propagating HOMs in those rectangular WGs will be broadband and will have multimode character, the WGs sharp corners are blended (r = 5 mm) to avoid possible EM field concentration at the sharp corners that can introduce heat load or discharges and consequently a quench.

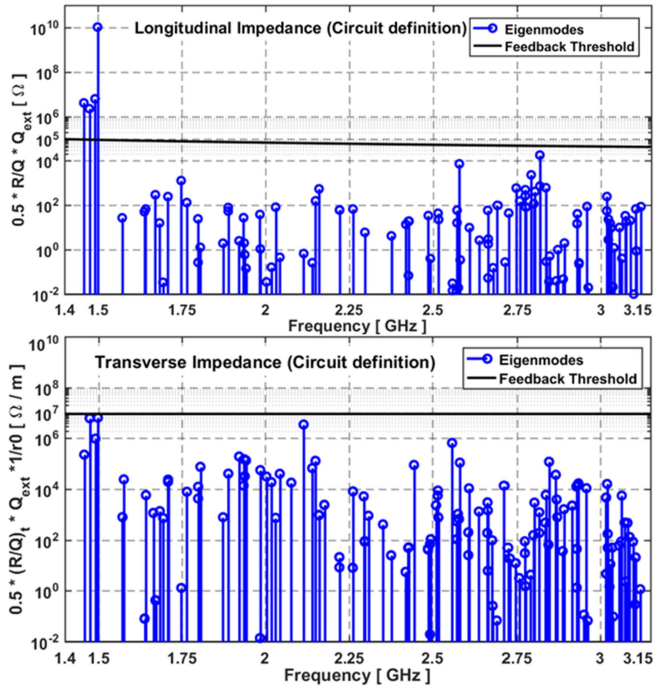

Fig. 11. Longitudinal (top) and transverse (bottom) impedances of the 1.5 GHz cavity.

To obtain a first detailed view of the impedance spectrum below 3 GHz accurate eigenmode simulations are performed using CST [26]. In the simulation model, all ports were activated and defined as waveguide ports with 10 modes each to ensure proper mode damping in the simulation at different frequencies, i.e., accurate estimation of Q_{ext} of the given mode. In Fig. 11, the longitudinal and transverse impedance of the 1.5 GHz cavity resonant modes are presented. It can be seen how the waveguide-loaded end-groups and enlarged beampipes provide proper damping and the feedback threshold is not exceeded.

As expected, only the fundamental TM_{010} π-mode and the rest of the fundamental pass-band modes exceed the impedance threshold and cannot be handled by an active feedback system. Although the first three monopole modes have very low R/Q in comparison with the AM, they can be strongly excited by a circulating high current beam due to the very low losses of the SRF cavity. Thus, these modes should be considered for beam loading. A detailed study is presented in [27]. As these Lower Order Modes (LOMs) have very high $Q_{ext} \sim 10^7$–10^8 related to the FPC coupling of the accelerating π-mode and are not considered for active operation, the resonant frequencies of LOMs should not hit any of the beam harmonics defined as multiples of the 1.25 MHz revolution frequency. Hence, for

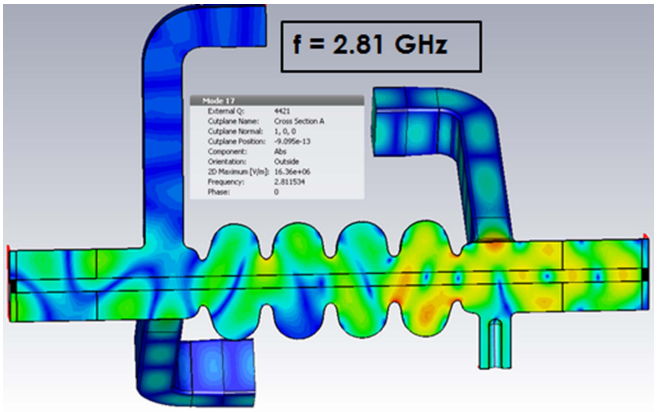

Fig. 12. Electric field of the 1.5 GHz cavity HOM with resonant frequency of 2.81 GHz.

every cavity design with perfectly tuned accelerating π-mode, the LOMs off-resonant condition should be fulfilled as well. As can be seen in Fig. 11, both the longitudinal and transverse impedance budgets are fulfilled. Nevertheless, some longitudinal and transverse HOMs are close to the feedback threshold and require special attention in beam dynamics studies [1], [25]. As a result, these modes can be handled by an active feedback system and are not critical as long as they are off-resonance with the circulating beam harmonics.

As it is proven by literature, the cavity resonant modes can be calculated very accurately with the application of eigenmode simulations. Nevertheless, this kind of simulation becomes very sensitive on the port boundaries at the resonant frequencies above a certain limit and in the case of the VSR cavity above about 3 GHz. As an example, Fig. 12 presents the electric field amplitude of the cavity HOM at 2.81 GHz, illustrating the strong coupling of the fields inside the cavity with both the beampipe and the waveguide extensions.

It is well known that the density of the cavity resonant spectrum drastically increases at higher frequencies and resonant modes can freely propagate through the different ports. As a result, the eigenmodes simulations become very expensive and inaccurate. Hence, eigenmode simulations are very powerful tools for accurate estimation of the cavity resonant modes but are limited to modes above 3 GHz for multi-cell cavities. Nevertheless, one cannot discard the presence of dangerous modes at higher frequencies and in particular, modes coinciding with the different multiples of the circulating beam harmonics. In order to calculate the cavity HOMs at higher frequencies up to 20 GHz, the application of long-range wakefield simulations is required and is discussed in the next section being part of the design stages 3 and 4 (Fig. 5).

V. Wakefield Simulations and Cavity HOM Spectrum Control

To estimate the excitation of HOMs in each cavity up to 20 GHz, long-range (20 m) wakefield simulations with a $\sigma = 4$ mm (-13 ps) bunch are performed using CST Studio Suite [26]. In this setup, the number of mesh cells is about 900 million and is close to the software limit. In these simulations, port boundaries were used to model the extraction of the EM field energy from the system. The accurate simulation of this class of EM problems requires proper modeling of HOM energy extraction from the system and requires multimode port modeling as the main HOM field extraction mechanism for the SRF cavities. Then the obtained wake potential is used to extract the resonant frequency and Q_{ext} by application of the Prony–Pisarenko pole-fitting technique [28]. Based on this technique a postprocessing MATLAB tool was developed to perform the fitting of the time domain signal to the sum of periodic signals with exponential damping, i.e., wake potential representation by means of superposition of cavity eigenmodes and reads

$$W\ (s) = 2\sum_i K_{loss,i} \cdot \cos\left(\frac{\omega_i}{c}s\right) e^{-\alpha_i s} \tag{4}$$

where c is the speed of light, $K_{loss,i}$ and $\alpha_i = \omega_i\ /(2cQ_L)$ are the loss factor and attenuation constant of ith resonant mode with angular frequency ω_i. Good agreement between the reconstructed and original wake potentials is achieved and shown in Fig. 13.

This technique represents a powerful tool for a broad scan of the most representative impedance sources in high-frequency ranges. It must be noted that since beam effects are included, the obtained spectrum accurately describes the spectrum of dangerous modes whereas eigenmode calculations carry the risk of missing unresolved modes by the solver. In Fig. 13, the most prominent resonant mode impedances interacting with the bunch are presented. This technique allows estimation of the HOMs up to 20 GHz and validates the impedance of the design to be lower than the feedback threshold as depicted in the lower part of Fig. 13. The accuracy of this method is sensitive to the simulated wake potential length, requiring proper mode damping in the time domain. Thus, for this particular SRF cavity design with strong HOM damping, the simulated 20 m long wake potential covers significant HOM damping ($Q_L \leq 2000$) of the time domain signal, which is essential for the accuracy of the pole-fitting technique. It must be noted that 20 m of wake simulation length covers a time span of -67 ns, which results in a frequency resolution of 15 MHz.

Resonances of significantly smaller line widths are likely to remain undetected in the impedance spectrum. If high Q values were to be extracted ($Q_L \sim 10^7$–10^8, i.e., of monopole-band modes) the long-range wake potential should contain the appropriate decay rate of those modes and would require wake lengths of more than 100 km to be simulated which is unrealistic. Thus, this technique offers very poor accuracy for nondamped monopole-band modes. Nevertheless, these modes can be calculated with high accuracy using an eigenmode solver.

Having identified the modes that lay dangerously close to the circulating beam harmonics the next step is to tune the HOM response to avoid any cause for beam loss. By the presented technique, it is then possible to control the cavity HOM spectrum during cavity design to some extent. This is done by making use of the spectral response of the wake potential in the mean of a fast Fourier transformation (FFT). It gives a first estimate of

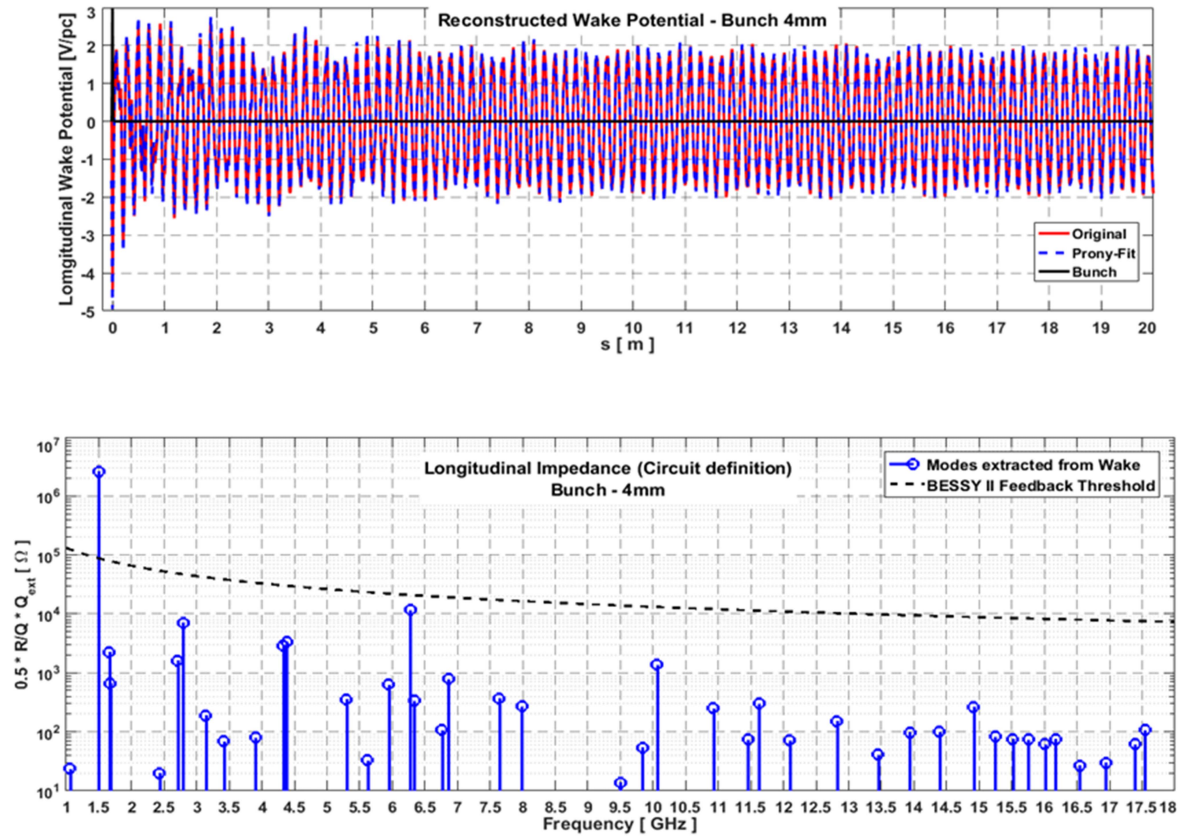

Fig. 13. Long-range wake potential (top) and impedances (bottom) computed by pole fitting technique.

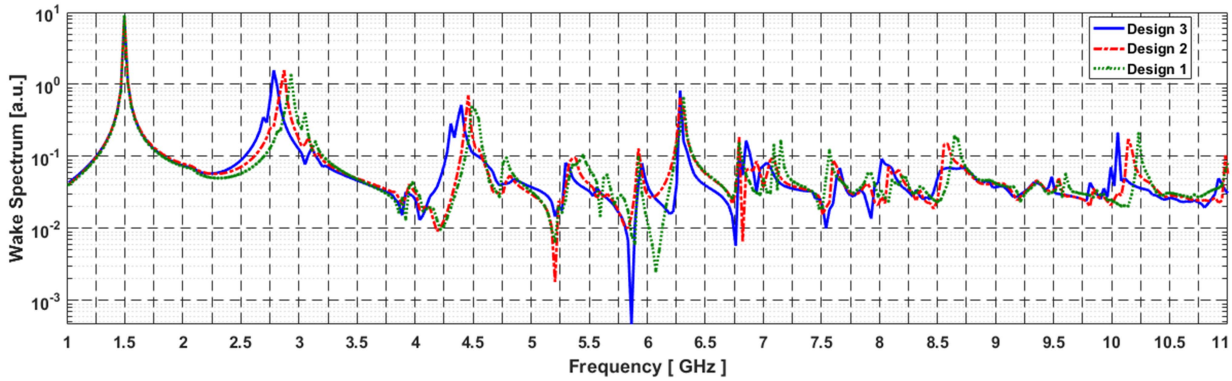

Fig. 14. Broadband HOM spectrum of the 1.5 GHz cavity for three different designs.

the most prominent resonant frequencies and their distance to the beam harmonics (multiple of 250 MHz). Then, the precise R/Q and Q_L values of the most prominent resonant modes interacting with the beam are calculated using a pole-fitting technique.

To demonstrate the cavity HOM spectrum shift, three different 1.5 GHz cavity designs are chosen with spectrums presented in Fig. 14. Out of many cavity designs, these (Table VI) are chosen to illustrate the HOM spectrum shift. Their modified geometry parameters with respect to parameters given in Table IV are presented in Table VI. The accelerating TM_{010} π-mode in all these designs is perfectly tuned according to the design goals as presented in Table V. In general, the cavity design is an optimization process consisting of seven geometry parameters. Therefore, to illustrate the HOM optimization the different steps are described next.

Starting from Design 1, the following optimization steps (see Fig. 5) are applied.

1) Tuning of the HOM spectrum: Change $A_{\text{mid-cup}}$ in the mm range and find the corresponding $A_{\text{end-cup}}$ for the AM field flatness. As a side effect, the AM frequency is shifted.

TABLE VI
GEOMETRY PARAMETERS VARIED FOR DIFFERENT BESSY VSR 1.5 GHZ CAVITY DESIGNS FOR HOM SPECTRUM SHIFT

Parameter [mm]	Design 1	Design 2	Design 3
R_{eq}	92.20	91.09	90.00
$A_{mid\text{-}cup}$	33.0	35.5	38.0
$A_{end\text{-}cup}$	30.4	32.7	35.0

TABLE VII
DESIGN STEPS FROM CAVITY DESIGNS 1 TO 2

Sequence	Parameter changes in [mm]		AM - Δf [MHz]	FF [%]
Step 1	$A_{mid\text{-}cup}$	33 → 35.5	−15	57
Step 2	$A_{end\text{-}cup}$	30.4 → 32.7	−20	96.8
Step 3	R_{eq}	92.2 → 91.1	0	98.7

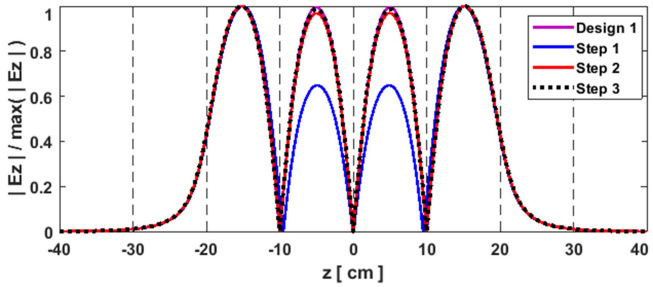

Fig. 15. On-axis electric field amplitude along the 1.5 GHz cavity at different design optimization steps.

2) Tune the AM frequency back to meet the specifications by adjusting R_{eq} (mm range) and checking the field flatness.
3) Fine-tuning of the AM field flatness and frequency by adjusting $A_{end\text{-}cup}$ and R_{eq} (sub-mm range), respectively.
4) Check the AM peak fields and tune on demand by geometry parameter set {a, b, B}. Then, repeat the fine-tuning step.
5) Check the HOM spectrum.

The sequence of the applied geometrical changes to the cavity surface and their influence on the AM fundamental frequency as well as the field flatness values are presented in Table VII. The last optimization Step 3 already corresponds to Design 2.

The electrical field profiles at different optimization steps are presented in Fig. 15. The field flatness is not so sensitive to the equator radius (R_{eq}) changes used for tuning the AM frequency and mainly depends on the geometry parameter ratio $A_{end\text{-}cup}/A_{mid\text{-}cup}$. This geometry parameter ratio $A_{end\text{-}cup}/A_{mid\text{-}cup} \sim 0.92$ is the same for all designs in Table VII offering field flatness preservation higher than 95%.

In Fig. 16, the HOM spectrums corresponding to the different optimization steps of the cavity design are presented. Since the AM frequency tuning (Step 3) shifts some of the HOM frequencies significantly, it is reasonable to compare the HOM spectrums of different cavity designs with a perfectly tuned AM satisfying the design goals (Table III). For example, it can be seen, that for Design 2 one of the HOMs with a frequency around 4.5 GHz is close to the beam harmonic line (Fig. 16). Consequently, the described optimization procedure is repeated to reach cavity Design 3 from Design 2.

It must be noted that the frequency detuning of the different HOMs (Fig. 14) is not linear or proportional as it depends on the type of modes and field distribution. It can be easily inferred that for some HOMs in the vicinity of 2.75 GHz and 8.5 GHz, the frequencies are shifted more than at around 6.25 GHz. Due to the different HOM frequency shift rates, shifting the one mode frequency far from beam harmonic lines could lead to a closer distance of a different mode to another harmonic line. Thus, the complete fulfillment of the off-resonance condition for all HOMs in a broad frequency range becomes a difficult task and folds into the search for an optimum cavity design with HOM frequencies at least by 50 MHz off-resonance. A detailed study shows that for a perfectly tuned fundamental mode, the parameter sensitive for the HOM spectrum shift can be expressed in terms of a cavity geometry single parameter: the mid-cell slope α (Fig. 6) connecting the iris and the equator of the cells. Thus, by changing the mid-cell slope α, the cavity HOM spectrum is successfully shifted away from the beam harmonics shown in Fig. 14 (vertical dashed lines). Therefore, the set of parameters, R_{eq}, $A_{mid\text{-}cup}$, and $A_{end\text{-}cup}$ (α) give the maximum HOM tailoring possibilities with minimum impact on the fundamental passband.

Finally, Design 3 is reached (Fig. 14) representing the best option studied in terms of the cavity broadband HOM spectrum up to 11 GHz which fulfills the off-resonance condition with beam harmonics being apart by at least 50 MHz. Note, that the HOM spectrum estimated by FFT of long-range wake potential resolves the most prominent HOMs with relatively high shunt impedances that are interacting with the bunch. Thus, to complete the cavity design (Fig. 5), the final step demands the use of eigenmode analyses (< 3 GHz) and pole-fitting technique (> 3 GHz) for accurate calculation of the cavity mode atlas for Design 3 and to ensure that HOM impedances are below the feedback threshold (Figs. 11 and 13) of the BESSY II storage ring.

In Fig. 17, the wake potential spectrums obtained from the optimizations of both the 1.5 GHz and 1.75 GHz cavity designs are presented. The wake spectrum is not hitting any of the beam resonances, which are located at a multiple of 250 MHz, as the most prominent ones for the "Baseline" filling pattern.

The individual cavity spectrum is important for investigating the source of HOMs during cavity operation in the storage ring, as other surrounding accelerator components are also potential impedance sources [15], [16], [17].

A. Limitations in Tuning by Number of Cells

When designing a multi-cell SRF cavity for storage ring operation with a controlled HOM spectrum, the number of cavity cells is one of the limiting factors as every resonant mode of the

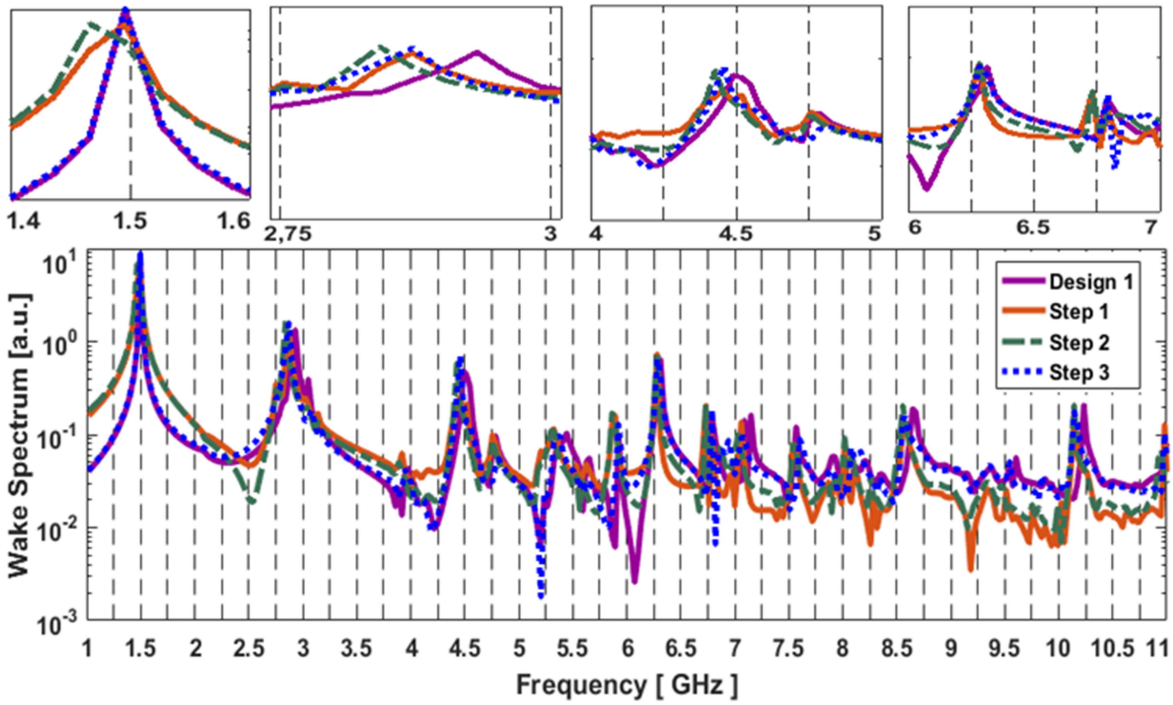

Fig. 16. Broadband HOM spectrum of the 1.5 GHz cavity at different design optimization steps. The zoom of the spectrum is around 1.5 GHz, 2.8 GHz, 4.5 GHz, and 6.5 GHz frequencies (top row).

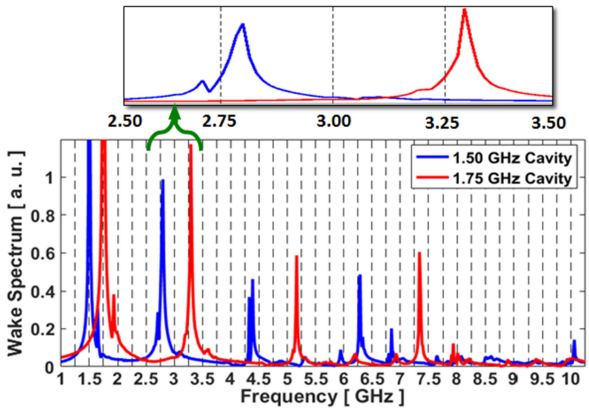

Fig. 17. Longitudinal wake spectrum of 1.5 GHz (blue) and 1.75 GHz (red) cavities. Vertical dashed lines represent the beam harmonics as multiples of 250 MHz.

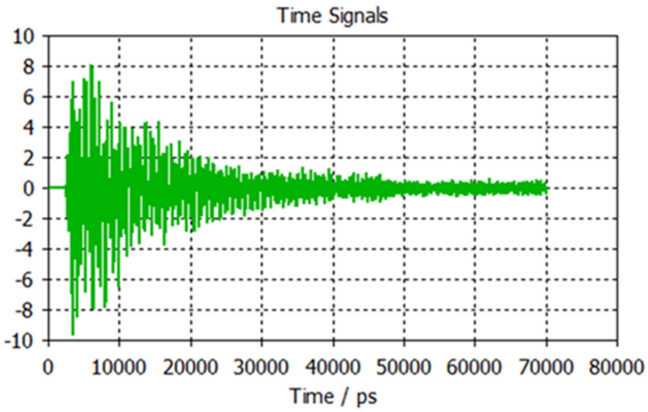

Fig. 18. Simulated power signal of the first mode of the waveguide port.

single cell starts to split into several modes defined by the number of cells. This results in a dense HOM spectrum, i.e., it reduces the frequency spacing between the cavity's resonant modes and makes it more difficult to shift HOMs away from beam harmonic lines. During the design of the BESSY VSR cavities, it was observed that the HOM frequencies were not shifted with equal portions for different designs and were efficiently optimized for the BESSY VSR multi-cell cavities with up to five cells. By increasing the number of cavity cells, the HOM frequency separation gets smaller making the broadband HOM spectrum control more difficult during cavity design. Note that for single bunch operation, the beam harmonics are multiples of the revolution frequency (1.25 MHz in the case of the BESSY II). Thus, it is impossible to fulfill the off-resonance condition since the HOMs at higher frequencies do have not enough separation between each other.

VI. HOM Power Levels for BESSY VSR Filling Pattern

The CST wakefield simulations discussed in the previous section, calculate the power signals at every port mode (Fig. 18). These signals corresponding to single bunch excitation are evaluated in postprocessing to estimate HOM power levels to be extracted from the system for bunch filling pattern of BESSY VSR.

For the simulation to be consistent, the total energy losses in the simulated system should not exceed the EM energy excited by the bunch in the system. This necessary condition reads as

follows:

$$W_b \geq W_{heat} + \sum_i \sum_n W_{i,\,n}^{Port} \tag{5}$$

where $W_b = q^2 \times K_{loss}$ is the energy excited by the bunch calculated from the K_{loss} loss factor, W_{heat} is the losses on the structure walls and dielectric parts, and the $W_{i,n}$ is the EM energy flown through the ith mode of the nth port of the cavity and can be calculated from power signals of the port S_p as follows:

$$W_{i,\,n}^{Port} = \int_0^{T_s} \left(S_p\left(i,n,t\right)\right)^2 dt\,. \tag{6}$$

Since the BESSY VSR cavities are superconducting the extraction of the EM energy from the system occurs primarily through the ports, i.e., excited HOMs are damped through the different ports. Particularly, for the above-mentioned 1.5 GHz SRF cavity the total EM energy flowing out through all ports is $W_p = 1.47\ \mu J$ while the energy lost by the beam into the system is $W_b = 2.27\ \mu J$. Thus, the condition of the energy balance (5) is fulfilled. The remaining EM energy corresponds to the excited monopole band modes that are not damped. Among those, the main energy is concentrated in the AM as it has the highest R/Q, i.e., the bunch interacts with the accelerating π-mode stronger than with other resonant modes of the cavity. This can be seen in wake potential as well, where the HOMs are damped very fast, and the remaining periodic wake potential corresponds to the AM (Fig. 13).

This type of simulation contains also information on HOM power levels, spectrum, and modal distribution at each port. This is important for special RF load optimization with broadband and multimode-absorbing properties [20]. The spectral power levels of the stored beam (filling pattern) are estimated by applying the spectral weighting technique to each port signal given as follows:

$$P\ (\omega) = \left| \frac{\tilde{I}_b\left(\omega\right)}{\tilde{I}_0\left(\omega\right)} \cdot \mathcal{F}\left(\omega\right) \right|^2 \tag{7}$$

where $\tilde{I}_0(\omega)$ and $\tilde{I}_b(\omega)$ are the current spectrums of the simulated single bunch and the stored bunch train, respectively. The function $\mathcal{F}(\omega)$ is the spectrum of the time signal belonging to each mode at a given port. Assuming Gaussian charge distribution for every bunch in the train, the $\tilde{I}_b(\omega)$ current spectrums can be presented analytically as follows:

$$\tilde{I}_b\left(\omega\right) = \sum_n I_n \cdot e^{-0.5\cdot\omega^2\sigma_n^2} \cdot\ e^{j\ \omega\ t_{0,n}} \tag{8}$$

where $I_n = q_n\ /T_{rev}$ is the current of the nth bunch in the train with total charge q_n and time position $t_{0,n}$ within revolution time T_{rev}. Note that the weighting technique takes into account the phase (position) of each individual bunch in the train and in case of hitting even a single beam harmonic will be reflected in the power level and observed in the spectrum. The signal spectrum $\mathcal{F}(\omega)$ is computed by FFT ensuring the preservation of the total energy calculated in time and frequency domains and reads

$$\frac{1}{2}\int_0^{\infty} \mathcal{F} * \mathcal{F}^*\, d\omega = \int_0^{T_s} S_p^2\, dt\,. \tag{9}$$

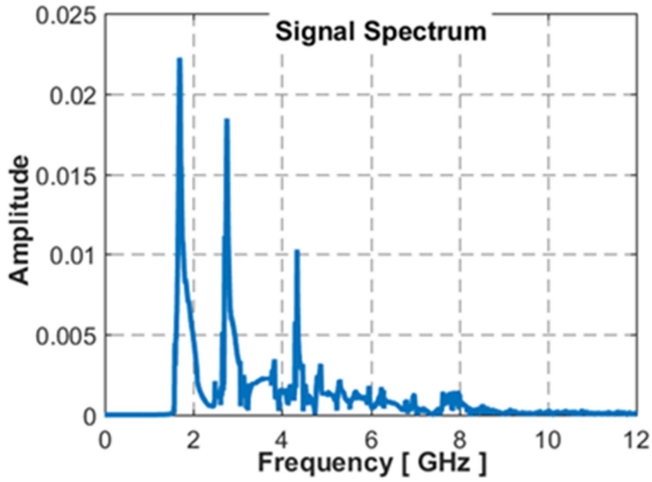

Fig. 19. Power signal spectrum corresponding to the time signal Fig. 18 with 1.25 MHz sampling rate.

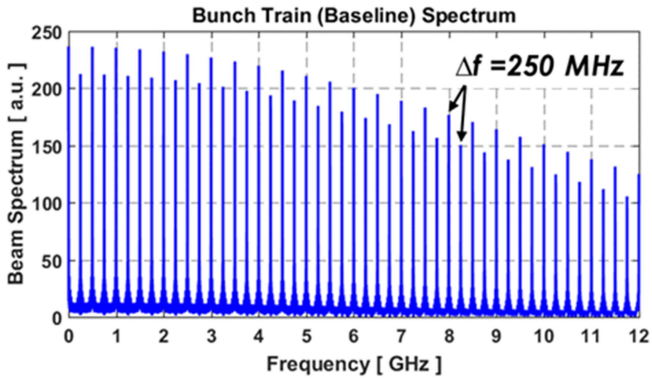

Fig. 20. Bunch train current spectrum for "Baseline" filling pattern.

Since the time signal has a limited length, the direct FFT results in coarse frequency sampling determined by the signal length. However, for accurate HOM power calculations $\mathcal{F}(\omega)$, the frequency sampling of 1.25 MHz revolution frequency of the BESSY II ring is required. This can be achieved by interpolating the directly obtained signal spectrum. A spline or Gaussian interpolation is applied at every frequency sampling point to resolve possible cavity resonant HOM frequencies that are closely spaced. Note that the resampled $\mathcal{F}(\omega)$ requires additional normalization to fulfill the necessary condition (9). An equivalent approach is to extend the time signal to the revolution time 800 ns of the BESSY II ring by just adding zero values resulting in the $\mathcal{F}(\omega)$ frequency sampling points multiple to 1.25 MHz. However, it is applicable only when the time signal is long enough and is damped strongly to be nearly zero like in Fig. 18.

As an example, the signal spectrum corresponding to the time signal (Fig. 19) is presented. The complete procedure implies following the same procedure for every power signal from the wakefield simulation.

The bunch train spectrum for the "Baseline" filling pattern is presented in Fig. 20 indicating the strong beam harmonics multiple of 250 MHz.

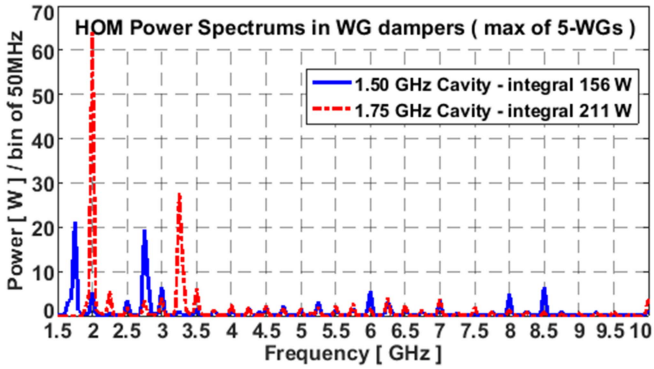

Fig. 21. HOM powers in WG-dampers obtained for "Baseline" filling pattern.

TABLE VIII
HOM POWER LEVELS FOR "BASELINE" FILLING PATTERN

Cavity type	1.5 GHz	1.75 GHz
Port no.	HOM power [W]	
1 – FPC(1)	38	34
2 – WG(1)	105	155
3 – WG(1)	104	152
4 – WG(2)	89	108
5 – WG(2)	90	110
6 – WG(2)	91	112
7 – BmP(Upstream)	236	201
8 – BmP(Downstream)	327	276
Total power		
"Coherent"	1080	1148
"Non-Coherent"	1293	1300

One of the fast indications of the fulfillment of the off-resonance condition between the cavity HOM spectrum and the beam harmonics is the comparison of so-called "Coherent" and "Non-Coherent" HOM powers. The "Coherent" HOM power takes into account the individual bunch phase in the train, while in the "Non-Coherent" one the phase is omitted [last exponential term in (8)], i.e., is considered as the sum of powers of each individual bunch separately. In the case when one of the HOM frequencies is closer to the beam harmonic the "Coherent" power will be higher than the "Non-Coherent" one. Then this dangerous frequency will be indicated also in the HOM power spectrum.

In Fig. 21, the expected HOM power spectrum for each cavity is presented and indicates the highest power level defined as the maximum of the five WG loads at a given frequency. The power spectrum contains also information on mode distribution at every frequency used for RF load optimization [20].

In Table VIII, the total HOM powers at each port of individual cavities are presented. In the table, the ports are grouped in two end-grouped given by upper index (1, 2).

Note that the presented power levels (Table VIII) are evaluated for the cavities with HOM spectrum (Fig. 17) that are not hitting any of the beam harmonics. In case of hitting one of the beam harmonics, the power levels can be easily doubled with a significant power increase at those resonant frequencies.

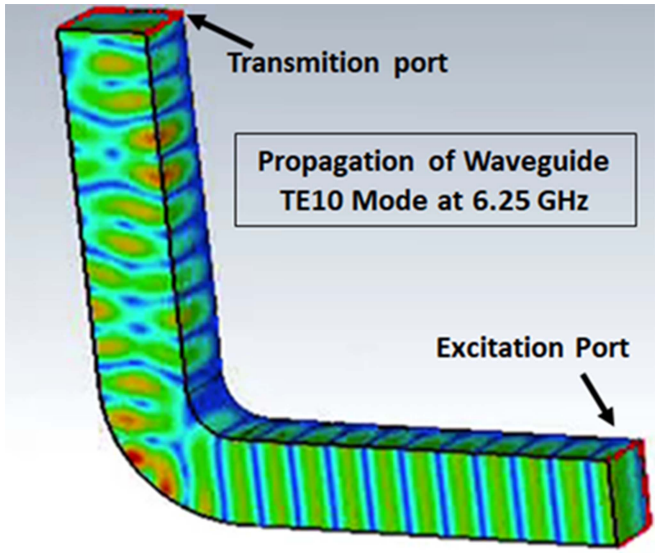

Fig. 22. Electric field of waveguide 90°-bend for TE_{10} waveguide mode propagation at 6.25 GHz.

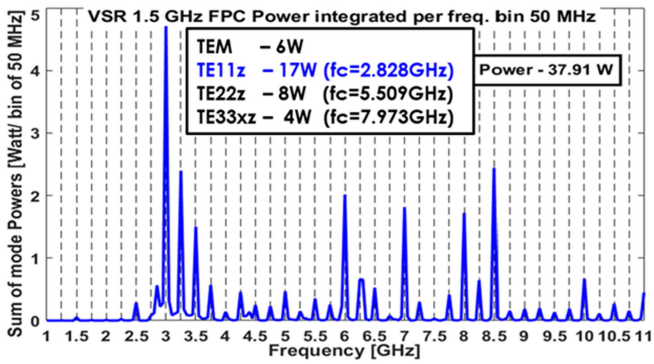

Fig. 23. HOM power in FPC port obtained for "Baseline" filling pattern.

As part of the cavity design, the radius of the HOM waveguide 90° bend (Figs. 4 and 10) was optimized for low reflection in the broadband frequency range up to 8 GHz, and the broadband reflection below 10% for propagating waveguide modes is achieved. It results in a 30 mm inner bending radius as optimum in terms of multimode waveguide mode excitation. At higher frequencies when other waveguide modes can be excited, the waveguide bend acts as a mode mixer, i.e., the single propagating mode couples to several waveguide modes after bend (Fig. 22). This phenomenon was considered in HOM load design [20] and is based on the coupling of the cavity HOMs to the waveguide modes after the bend.

Another dimensional optimization was performed for the coaxial port for the FPC. The optimization criteria for the coaxial dimensions were defined for the HOM power level at the FPC port to not exceed 100 W. In Fig. 23, the power modal and spectral distribution at the FPC port are shown.

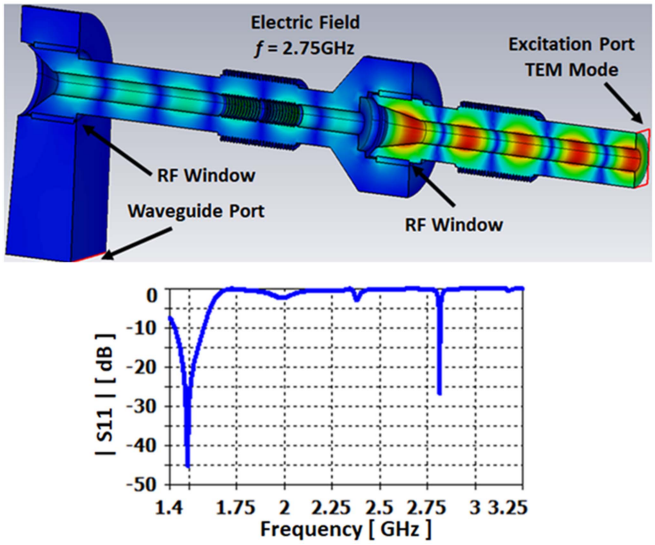

Fig. 24. Electric field (top) of the FPC at 2.75 GHz excitation on coax TEM mode and the S11 magnitude versus frequency (bottom) for the same excitation.

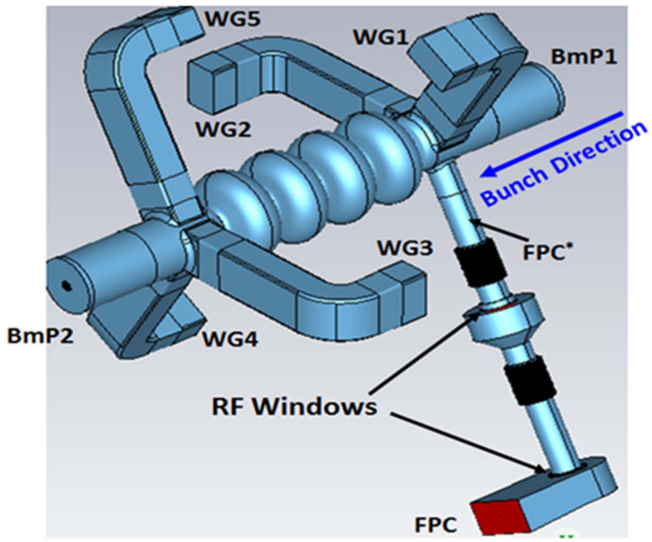

Fig. 25. Simulation model of the waveguide-damped four-cell VSR cavity with integrated full FPC.

As can be seen the HOM power at the FPC port is mainly concentrated at the higher coaxial mode TE_{11} while the cavity will be driven by the TEM mode. Hence, to protect the RF windows that are part of the FPC design [29], [30], [31], [32], the coax dimensions of both couplers cold parts are optimized to decouple the HOMs and push those powers more into the WG-dampers. The final FPC port coax parameters (outer and inner diameters) are 49 × 20 mm and 42 × 18 mm for 1.5 GHz and 1.75 GHz cavities, respectively. The BESSY VSR input coupler design is a coaxial-type high-power coupler derived from the Cornell injector coupler for the ERL [33].

To investigate the impact of the HOM power on the FPC cold ceramic window, the frequency domain simulations for the complete FPC model were performed. The model and simulation setup are presented in Fig. 24. It consists of two coaxial lines

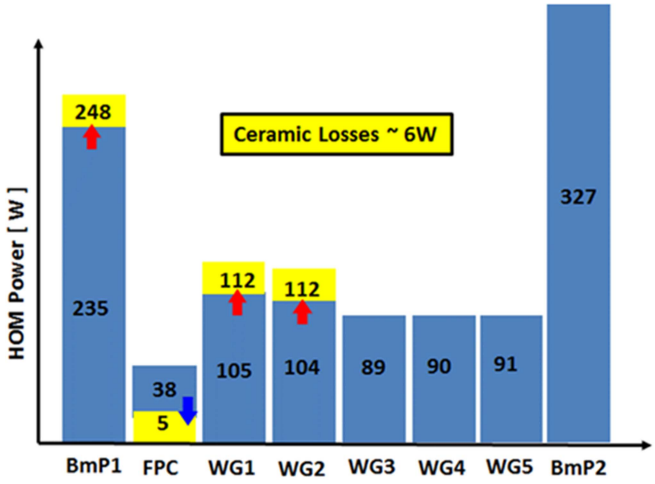

Fig. 26. HOM power distribution across 1.5 GHz cavity ports for models with (yellow) and without (blue) FPC, corresponding to the "Baseline" filling pattern.

TABLE IX
PROPERTIES OF MONOPOLE BAND MODES OF 1.5 GHZ CAVITY

Frequency [GHz]	R/Q [Ω]	Q_{ext}	Mode type
1.49866	386	$5.0 \cdot 10^7$	π
1.49134	0.41	$3.0 \cdot 10^7$	2π/3
1.47424	0.1	$4.7 \cdot 10^7$	π/2
1.45785	0.05	$16.0 \cdot 10^7$	2π

connected through the transition part where the cold RF window is located and the transition to the rectangular waveguide part with the warm RF window. Note that the model is perfectly tuned for the fundamental frequency transmission in coax TEM mode.

In Fig. 24 (bottom), the simulated reflection coefficient in the broad frequency range up to 3 GHz is presented. To simulate the cross coupling of the modes at high frequencies, in every port, five port modes are activated. As can be seen (Fig. 23) at higher frequencies, the waves are mainly reflected back from the cold RF window, i.e., forming a standing wave pattern. This can cause additional heat load on the RF window and an impedance increase on the cavity side. Thus, a wakefield simulation of the cavity with a full FPC model integrated (Fig. 25) was performed. The RF properties of monopole-band modes of the 1.5 GHz cavity (Fig. 25) are summarized in Table IX and considered for beam loading studies in [27].

In the HOM power diagram (Fig. 26) the power distributions at different ports for the models with and without FPC are presented.

As was expected, the HOM power at the FPC port is mainly reflected from the cold RF window. This reflected power is redistributed within the neighboring two waveguides and beampipe ports. There is no significant impact on the HOM impedance observed due to this phenomenon as the RF windows cause stronger impedance decoupling and push this additional power into neighboring ports.

VII. Conclusion

In this article, the successful optimization of the HOM spectrum for the BESSY VSR cavities in order to mitigate the risk of beam loss due to impedances is presented. The applied advanced optimization technique opens a door to include the control of broadband HOM spectrum as a fundamental part of the SRF cavity design specifications, which is essential for stable operation in storage rings and Linacs with high repetition rates. This approach has some limitations since the sensitivity of the different modes to the parameter α (cell slope) is not linear and highly depends on the mode field configuration. Nevertheless, the results obtained for the studied cavity have shown a high level of sensitivity for all modes considered dangerous for operation in the BESSY II synchrotron and suggest that a similar approach could be successfully applied to any type of elliptical cavity. To overcome the intrinsic frequency limitations offered by standard eigenmode-based approaches an alternative analysis based on pole fitting is applied for the first time to the cavity design as a robust and reliable solution. The application and limitations of different numerical techniques for the evaluation and control of the HOM spectrum of the cavities are discussed as compared to the proposed approach. For the VSR cavity, the fulfillment of the specifications for both the fundamental passband and the HOM broadband spectrum over an ultrawide frequency range of up to 20 GHz has been successfully demonstrated. The upper-frequency limit is defined by the limitations on the bunch length in the wakefield simulations. The conventional numerical methods implemented in most commercial software have limitations for short-bunch simulations due to the so-called numerical dispersion effect, which leads to significant degradation in simulation accuracy and convergence. Additionally, the developed technique offers several advantages that become useful for further stages of module analysis. For example, all the cavity spectrums obtained can be further used for the calculation of HOM power levels excited by the different bunch filling patterns in the storage ring and thus help to determine the most suitable arrangement of the four-cavity BESSY VSR module [14], [15], [16]. Currently, the 1.5 GHz prototype SRF cavities are in the production stage and further full commissioning of the system is foreseen.

References

[1] A. Jankowiak et al., *Technical Design Study BESSY VSR*. Berlin, Germany: Helmholtz-Zentrum, 2015.

[2] A. Jankowiak et al., "The BESSY VSR project for short X-ray pulse production," in *Proc. 7th Int. Part. Accel. Conf.*, May 2016, pp. 2833–2836.

[3] G. Wuestefeld, A. Jankowiak, J. Knobloch, and M. Ries, "Simultaneous long and short electron bunches in the BESSY II storage ring," in *Proc. 2nd Int. Part. Accel. Conf.*, Sep. 2011, pp. 2936–2938.

[4] N. Wunderer et al., "VSR demo cold string: Recent developments and manufacturing status," in *Proc. 20th Int. Conf. RF Supercond.*, Jun. 2021, pp. 647–651.

[5] P. Marchand et al., "Operational experience with the SOLEIL superconducting RF system," in *Proc. 16th Int. Conf. RF Supercond.*, Sep. 2013, pp. 627–631.

[6] J. M. Byrd et al., "Transient beam loading effects in harmonic RF systems for light sources," *Phys. Rev. Special Topics - Accelerators Beams*, vol. 5, 2002, Art. no. 092001.

[7] P. Marchand, "Superconducting RF cavities for synchrotron light sources," in *Proc. 9th Eur. Part. Accel. Conf.*, Jul. 2004, pp. 21–25.

[8] Y. C. Hsu, M.-C. Lin, M.-K. Yeh, and C.-L. Wu, "Optimization of a 1.5-GHz two-cell SRF cavity," *IEEE Trans. Appl. Supercond.*, vol. 29, no. 5, Aug. 2019, Art. no. 3500205.

[9] Z.-K. Liu et al., "Performance simulation for a prototype 1.5 GHz superconducting harmonic cavity," *IEEE Trans. Appl. Supercond.*, vol. 29, no. 5, Aug. 2019, Art. no. 3500505.

[10] T. Yanagisawa et al., "1500 MHz passive cavity for bunch lengthening in the NSLS-II storage ring," in *Proc. Part. Accel. Conf.*, 2009, pp. 2086–2088.

[11] G.-M. Ma, Z.-T. Zhao, and J.-F. Liu, "Design of a higher harmonic cavity for the SSRF storage ring," *Chin. Phys. C*, vol. 32, no. 4, pp. 275–279, 2008.

[12] A. Velez et al., "HOM damping optimization design studies for BESSY VSR cavities," in *Proc. 6th Int. Part. Accel. Conf.*, 2015, pp. 2774–2776.

[13] A. Velez et al., "The SRF developments for BESSY VSR," in *Proc. 8th Int. Part. Accel. Conf.*, 2017, pp. 986–989.

[14] A. Tsakanian et al., "Study on HOM power levels in the BESSY VSR module," in *Proc. 8th Int. Part. Accel. Conf.*, 2017, pp. 982–985.

[15] A. Tsakanian et al., "HOM power levels in the BESSY VSR cold string," in *Proc. 9th Int. Part. Accel. Conf.*, 2018, pp. 2808–2811.

[16] H.-W. Glock et al., "Design of the beamline elements in the BESSY VSR cold string," in *Proc. 9th Int. Part. Accel. Conf.*, 2018, pp. 4123–4126.

[17] H. Wang et al., "Simulations and measurements of a heavily HOM-damped multi-cell SRF cavity," in *Proc. 22nd Part. Accel. Conf.*, 2007, pp. 2496–2498.

[18] F. Marhauser et al., "Status and test results of high current 5-cell SRF cavities developed at JLAB," in *Proc. 11th Eur. Part. Accel. Conf.*, Jun. 2008, pp. 886–888.

[19] R. Rimmer et al., "Recent progress on high current SRF cavities at JLAB," in *Proc. 1st Int. Part. Accel. Conf.*, May 2010, pp. 3052–3054.

[20] J. Guo et al., "Development of waveguide HOM loads for BERLinPro and BESSY-VSR SRF cavities," in *Proc. 8th Int. Part. Accel. Conf.*, May 2017, pp. 1160–1163.

[21] J. Sekutowicz et al., "Design of a low loss SRF cavity for the ILC," in *Proc. 20th Part. Accel. Conf.*, May 2005, pp. 3342–3344.

[22] N. Valles et al., "Seven-cell cavity optimization for Cornell's energy recovery linac," in *Proc. 14th Int. Conf. RF Supercond.*, Sep. 2009, pp. 538–542.

[23] B. Aune et al., "Superconducting TESLA cavities," *Phys. Rev. Special Topics - Accelerators Beams*, vol. 3, 2000, Art. no. 092001.

[24] H. Padamsee, J. Knobloch, and T. Hays, *Superconductivity for Accelerators*. New York, NY, USA: Wiley, 1998.

[25] M. Ruprecht, "Calculation of coupled bunch effects in the synchrotron light source BESSY VSR," M.S. thesis, Humboldt Universität, Berlin, Germany, 2014.

[26] SIMULIA, "CST Studio Suite," [Online]. Available: www.3ds.com

[27] A. Tsakanian et al., "Beam loading in the BESSY VSR cavities," in *Proc. 19th Int. Conf. RF Supercond.*, Jun. 2019, pp. 217–221.

[28] P. Thoma and T. Weiland, "Calculation of Q-factors of lossy resonators in the time domain using the Prony-Pisarenko approximation," in *Proc. Comput. Accel. Phys. Conf.*, Feb. 1993, vol. 297, pp. 66–73.

[29] E. Sharples, M. Dirsat, A. Velez, and J. Knobloch, "Design of high power 1.5 GHz input couplers for BESSY VSR," in *Proc. 8th Int. Part. Accel. Conf.*, 2017, pp. 978–981.

[30] E. Sharples, M. Dirsat, Z. Muza, A. Velez, and J. Knobloch, "Design development for the 1.5 GHz couplers for BESSY VSR," in *Proc. 19th Int. Conf. RF Supercond.*, Jun. 2019, pp. 795–799.

[31] E. Sharples-Milne, V. Dürr, A. Neumann, P. Echevarria, A. Velez, and J. Knobloch, "Final design studies for the VSR DEMO 1.5 GHz coupler," in *Proc. 12th Int. Part. Accel. Conf.*, 2021, pp. 2300–2303.

[32] E. Sharples-Milne, V. Dürr, S. Schendler, N. Wunderer, A. Velez, and J. Knobloch, "The 1.5 GHz coupler for VSR DEMO: Final design studies, fabrication status and initial testing plans," in *Proc. 20th Int. Conf. RF Supercond.*, Jun. 2021, pp. 652–656.

[33] V. Veshcherevich, I. Bazarov, S. Belomestnykh, M. Liepe, H. Padamsee, and V. Shemelin, "A high power CW input coupler for Cornell ERL injector cavities," in *Proc. 11th Int. Workshop RF Supercond.*, Sep. 2003, pp. 722–725.